Cell sorting capabilities as diverse as your applications

SONY

Little to no expression of angiotensin-converting enzyme-2 (ACE2) on most human peripheral blood immune cells but highly expressed on tissue macrophages

Authors: Xiang Song[1], Wei Hu[1], Haibo Yu[1], Laura Zhao[2], Yeqian Zhao[2], Xin Zhao[1], Hai-Hui Xue[1], Yong Zhao[1]*

Affiliations:

[1] Center for Discovery and Innovation, Hackensack Meridian Health, Nutley, NJ 07110 USA

[2] Tianhe Stem Cell Biotechnologies Inc. Paramus, NJ 07652 USA

***Corresponding author:**

Yong Zhao M.D., Ph.D.

Associate Scientist

Center for Discovery and Innovation

Hackensack Meridian Health

340 Kingsland Street

Nutley, NJ 07110 USA

Tel: 201 880 3460

E-mail: Yong.Zhao@HMH-CDI.org

This article has been accepted for publication and undergone full peer review but has not been through the copyediting, typesetting, pagination and proofreading process which may lead to differences between this version and the Version of Record. Please cite this article as doi: 10.1002/cytoa.24285

Abstract:

Angiotensin-converting enzyme-2 (ACE2) has been recognized as the binding receptor for the severe acute respiratory syndrome coronavirus 2 (SARS-CoV-2). Flow cytometry demonstrated that there was little to no expression of ACE2 on most of the human peripheral blood-derived immune cells including $CD4^+$ T, $CD8^+$ T, activated $CD4^+/CD8^+$ T, Tregs, Th17, NKT, B, NK cells, monocytes, dendritic cells, and granulocytes. There was no ACE2 expression on platelets and very low level of ACE2 protein expression on the surface of human primary pulmonary alveolar epithelial cells. The ACE2 expression was markedly upregulated on the activated type 1 macrophages (M1). Immunohistochemistry demonstrated high expressions of ACE2 on human tissue macrophages, such as alveolar macrophages, Kupffer cells within livers, and microglial cells in brain at steady state. The data suggest that alveolar macrophages, as the frontline immune cells, may be directly targeted by the SARS-CoV-2 infection and therefore need to be considered for the prevention and treatment of COVID-19.

Key terms: Angiotensin-converting enzyme-2 (ACE2); COVID-19; SARS-CoV-2, macrophages; immune cells; pathogenesis; lung

INTRODUCTION

The epidemic of a new coronavirus infectious disease (COVID-19) is wreaking havoc worldwide, caused by the severe acute respiratory syndrome coronavirus 2 (SARS-CoV-2). Angiotensin-converting enzyme 2 (ACE2), with a multiplicity of physiological roles such as a negative regulator of the renin-angiotensin system, has been recognized as the entry receptor for SARS-CoV-2 infecting host cells (1), which is similar to the SARS-CoV. Other potential host cellular entry receptors have been tested or proposed for the viral invasion such as TMPRSS2 (transmembrane protease, serine 2) or cathepsin B/L (2), CD147 (3), O-acetylated sialic acid (4), antibody-dependent enhancement (ADE) pathway (5), and CD26 (6). ACE2 may act as a limiting factor for viral infection at the initial stage (7). The ACE2 expression has been mainly distributed in microvilli of the intestine and renal proximal tubules, gallbladder epithelium, testicular Sertoli cells and Leydig cells, glandular cells of seminal vesicle and cardiomyocytes (8). The human respiratory system is primarily affected by the SARS-CoV-2 infection. Using the polyclonal anti-serum-based immunohistochemistry, the expression of ACE2 was reported on type II alveolar epithelial cells (9). However, a single cell-RNA profiling analysis showed that only 1.4% ± 0.4% of lung type II alveolar epithelial cells expressed ACE2 at RNA level (10). Additionally, clinical autopsies from SARS-CoV-infected patients demonstrated that there were major pathological changes in the lungs, immune organs, and small systemic blood vessels with vasculitis. The detection of SARS-CoV was primarily found in the lung and trachea/bronchus, but was undetectable in the spleen, lymph nodes, bone marrow, heart and aorta (11). This evidence highlights the overreaction of immune responses induced by viral infection which resulted in significant harm, as evidenced by pathogenesis of the lungs, immune organs, and

small systemic blood vessels. Similar mechanisms have been proposed in the pathogenesis for SARS-CoV-2 infection (12). The pathological study in COVID-19 patients revealed that the majority of infiltrated immune cells in alveoli were macrophages and monocytes, with minimal lymphocytes, eosinophils and neutrophils(13). Thus, there are fundamental knowledge gaps underlying the pathogenesis of COVID-19 that need to be clarified. To understand the immunopathology and advance the strategies for the prevention and treatment of COVID-19, we examined the levels of ACE2 expression on different types of immune cells. Our data demonstrated that the activated macrophages and alveolar tissue macrophages, among others, displayed high levels of ACE2, while most of the immune cells were negative or displayed very low expressions of ACE2. This data highlights the importance of macrophages in the pathogenesis and treatment of COVID-19.

MATERIALS AND METHODS

PBMC isolation

To detect the expression of ACE2 on different types of immune cells, human buffy coat blood units (N = 14; mean age of 49.07 ± 13.79; age range from 27 to 67 years old; 8 males and 6 females) were purchased from the New York Blood Center (NYBC, New York, NY, USA). NYBC has received all accreditations for blood collections and distributions including institutional review board (IRB) approval and signed Consent Forms from donors. Human buffy coats were initially added to 40 ml chemical-defined serum-free culture X-VIVO 15^{TM} medium (Lonza, Walkersville, MD, USA) and mixed thoroughly with 10 ml pipette. Next, they were used for isolation of peripheral blood-derived mononuclear cells (PBMC). PBMC were harvested as previously described (14). Briefly, mononuclear cells were isolated from buffy coats blood using

Ficoll-Paque^{TM} PLUS (γ=1.007, GE Healthcare, Chicago, IL, USA). Next, the red blood cells were removed using ACK Lysing buffer (Lonza, Walkersville, MD, USA). After three washes with saline, the whole PBMC were utilized for flow cytometry. To isolate monocytes, monocytes were purified from PBMC by using $CD14^+$ microbeads (Miltenyi Biotec, Bergisch Gladbach, Germany) according to the manufacturer's instruction, with purity of $CD14^+$ cells > 90%.

Flow cytometry

Phenotypic characterization of PBMC, monocytes, macrophages and Th17 cells were performed by flow cytometry with associated markers (Supplementary Table) including: PC5.5-conjugated anti-human CD3 mAb, ECD-conjugated anti-human CD3 mAb, Krome Orange-conjugated anti-CD8 mAb, APC-Alexa Fluor 750-conjugated anti-CD66b mAb, PC5.5-conjugated anti-human CD19 mAb, PC 5.5-conjugated anti-human HLA-DR mAb, Krome Orange-conjugated anti-CD14 mAb, APC-conjugated anti-human CD80, PE-conjugated anti-human CD123 mAb, PE-conjugated anti-human CD25 mAb, PE-Cy7-conjugated anti-human CD41 mAb, and FITC-conjugated anti-human CD42a mAb purchased from Beckman Coulter (Brea, CA, USA). The antibodies PB-conjugated anti-human CD3, and APC-conjugated anti-IL17A mAbs were purchased from Biolegend (San Diego, CA, USA). The antibodies APC-conjugated anti-human CD4 mAb, FITC-conjugated anti-human Hsp60 mAb, PE-Cy7-conjugated anti-human CD11c mAb, PE-Cy7-conjugated anti-human CD56 mAb, BV-421-conjugated anti-human CD127 mAb, PE-conjugated anti-RORγT, and BV 421-conjugated anti-RORγT mAbs, PE-conjugated anti-human CD163, and BV421-conjugated anti-human CD209 were purchased from BD (Franklin Lakes, NJ, USA). PE-conjugated anti-IL17F were purchased from Invitrogen (Carlsbad, CA,

USA). PE-Cy7-conjugated anti-human CD196 (CCR6) and PE-Cy7-conjugated anti-human MAVS mAbs were purchased from ThermoFisher Scientific (Waltham, MA, USA).

To detect an expression of ACE2 protein on different types of PBMC, macrophages, Th17 cells, platelets or platelet-derived mitochondria, the indirectly-labeled immunostaining with mouse anti-human ACE2 mAb (Novus Biologicals, Catalogue# NBP2-80035-100 µg, Clone #AC18F, Littleton, CO, USA) was utilized in combination with above lineage-specific fluorescence-labeled mAbs. Briefly, samples were first pre-incubated with human BD Fc Block (BD Pharmingen, Franklin Lakes, NJ, USA) to block non-specific binding for 20 minutes at room temperature, before being directly aliquoted for different antibody stainings. Cells were initially incubated with mouse anti-human ACE2 mAb at 1:50 dilution, at room temperature for 30 minutes. Next, cells were washed with PBS at 400 *g* × 5 minutes and then stained with FITC-conjugated AffiniPure donkey or Cy5-conjugated AffiniPure donkey anti-mouse 2nd Abs (Jackson ImmunoResearch Laboratories, West Grove, PA, USA) at 1:100 dilution for 30 minutes at room temperature. Cells only with 2^{nd} Ab staining served as control. After finishing the 2^{nd} Ab staining, cells were washed with 4 mL PBS to remove residual 2^{nd} Ab. Consequently, cells were immunostained with above lineage-specific fluorescence-labeled mAbs, as previously described (15-17). Staining with propidium iodide (PI) (BD Biosciences, Franklin Lakes, NJ, USA) was used to exclude dead cells during the flow cytometry analysis.

To detect ACE2 expression on human pulmonary alveolar epithelial cells, the freshly-isolated primary human pulmonary alveolar epithelial cells (HPAEpiC) were purchased from ScienCell Research Laboratories (Catalogue # 3200, Carlsbad, CA). Each vial contains $>1 \times 10^6$ cells in 1 ml volume from three healthy donors (2 females and 1 male). HPAEpiC were directly prepared for flow cytometry after being thawed, without *ex vivo* cultures.

For ACE2-positive control, the recombinant adenoviral vectors expressing human ACE2 (Ad5-hACE2) under the control of the CMV promoter was obtained from BEI resources (NR-52390). The ACE2 expression was performed as previously described(18-20). Briefly, HEK293T cells at confluency of 80~90% in 6-well plate were transduced with Ad5-hACE2 at a multiplicity of infection (MOI) = 0.5. After 24 hours post-infection, infected cells were harvested and stained with ACE2 antibody, followed by Flow Cytometry.

For intracellular staining, cells were fixed and permeabilized according to the PerFix-nc kit (Beckman Coulter, Brea, CA, USA) manufacturer's recommended protocol. After staining, cells were collected and analyzed using a Gallios Flow Cytometer (Beckman Coulter, Brea, CA, USA), equipped with three lasers (488 nm blue, 638 red, and 405 violet lasers) for the concurrent reading of up to 10 colors. The final data were analyzed using the Kaluza Flow Cytometry Analysis Software (Beckman Coulter, Brea, CA, USA).

Isolation of monocytes from PBMC and macrophage polarization

To generate monocyte-derived macrophages and detect ACE2 expression, monocytes were purified from human PBMC by using CD14 microbeads (Miltenyi Biotec, Bergisch Gladbach, Germany) according to the manufacturer's instruction, with the purity of $CD14^+$ cells > 90%. The isolated monocytes were seeded in the six-well tissue culture-treated plate at 5×10^5 cells/ well in 2 mL X-VIVO 15 serum-free culture media at 37 °C, 5% CO_2 condition. After 2-hour culturing, the attached monocytes were washed twice with PBS to remove floating cells and cellular debris, followed by treatment with 50 ng/mL M-CSF (14, 15) (Sigma, Saint Louis, MO, USA) in X-VIVO 15 serum-free media at 37 °C, 5% CO_2. After culturing for 7 days, the macrophages were treated with 1 μg/mL lipopolysaccharides (LPS) (Sigma, Saint Louis, MO,

USA) or 40 ng/mL IL-4 (Biolegend, San Diego, CA, USA) for M1 and M2 polarization respectively (21) for 24 hours in X-VIVO 15 serum-free medium. Consequently, cells from different groups were collected for evaluations. To detect the ACE2 expressions on M1 and M2 macrophages, the immunocytochemistry was performed as previously described (17). Briefly, M1 and M2 macrophages were fixed with 4% paraformaldehyde for 20 min at room temperature, blocked with 2.5% horse serum (Vector Laboratories, Burlingame, Ca, USA) and human BD Fc Blocker for 20 min at room temperature, and then immunostained with mouse anti-human ACE2 monoclonal antibody (Novus Biologicals, Centennial, CO USA) at 1:200 dilution for 2 hours at room temperature. Next, cells were stained with Cy5-conjugated AffiniPure donkey anti-mouse 2nd Ab (Jackson ImmunoResearch Laboratories, West Grove, PA, USA) at 1:100 dilution at room temperature for 1 hour. Only cells with 2nd Ab staining served as negative control. Finally, cells were mounted by using mounting medium with DAPI (Vector Laboratories, Burlingame, CA, USA) and photographed with a Nikon Eclipse Ti2 inverted microscope, using NIS Elements Version 4.60 software.

Immunohistochemistry

Paraffin tissue sections from normal adult humans (N = 8, aged from 21 to 87 years old, 3 males, 5 females) were purchased from BioChain Institute Inc (Catalog No: T8234431, Newark, CA, USA), including brain, lung, liver, spleen, and kidney tissue sections. Immunostaining was performed as previously described with minor modifications (22). To block non-specific staining, sections were incubated in a buffer containing 2.5% horse serum (Vector Laboratories, Burlingame, Ca, USA) and human Fc Block (BD Pharmingen, Franklin Lakes, NJ, USA) for 20 minutes at room temperature. Tissue sections were initially immunostained with anti-ACE2

rabbit polyclonal antibody (Abcam, Cambridge, MA, USA) and rat anti-human CD11b monoclonal antibody (mAb) (Biolegend, San Diego, CA, USA) at 1:100 dilution for 2 hours at room temperature. Next, tissue sections were stained with FITC-conjugated AffiniPure donkey anti-rat 2^{nd} Ab and Cy3-conjugated AffiniPure donkey anti-rabbit 2^{nd} Ab (Jackson ImmunoResearch Laboratories, West Grove, PA, USA) at 1:100 dilution at room temperature for 1 hour. For every experiment, only tissue sections with 2^{nd} Ab staining served as negative control. Finally, the slides were mounted by using mounting medium with DAPI (Vector Laboratories, Burlingame, CA, USA) and photographed with a Nikon A1R confocal microscope on a Nikon Eclipse Ti2 inverted base, using NIS Elements Version 4.60 software. DIC images were photographed with Photometrics CoolSNAP™ DYNO CCD camera.

Statistics

Statistical analyses were performed with GraphPad Prism 8 (version 8.0.1) software. The normality test of samples was performed by the Shapiro-Wilk test. Statistical analyses of data were performed by the two-tailed paired Student's t-test to determine statistical significance between untreated and treated groups. The Mann-Whitney U test was utilized for non-parametric data. Values were given as mean ± SD (standard deviation). Statistical significance was defined as $P < 0.05$, with two sided.

RESULTS

Little to no expression of ACE2 on most human peripheral blood-derived immune cells

To explore the direct action of SARS-CoV-2 on immune cells, we examined the ACE2 expressions on different types of immune cells from human peripheral blood (n = 14). They were characterized and gated with cell type-specific surface markers (23): $CD3^+$ for T cells, $CD3^+CD4^+$ for $CD4^+$ T cells, $CD3^+CD8^+$ for $CD8^+$ T cells, $CD11c^+CD14^-$ for myeloid dendritic cells (mDC), $CD14^-CD123^+$ for plasmacytoid DC (pDC), $CD14^+$ for monocytes, $CD19^+$ for B cells, $CD4^+CD25^+CD127^{low/-}$ for regulatory T cells (Tregs), $CD3^+CD56^+$ for NKT cells, $CD3^-CD56^+$ for NK cells, and $CD3^-CD66b^+$ for granulocytes (Figs. 1a-c). Using the recombinant adenoviral vectors expressing human ACE2 (Ad5-hACE2)-transfected 293T cells as positive control (20) (Fig.1d), flow cytometry demonstrated that there were no expressions of ACE2 on most types of immune cells, or with a background level (< 5%) (Fig. 1e-g). The percentages of $ACE2^+$ cells for NK and NKT cells were only 1.06% ± 1.22% and 2.01% ± 1.17% respectively (n = 11) (Fig. 1f), and 0.31% ± 0.27% for $ACE2^+CD4^+$ T cells. The activated $CD4^+$HLA-DR^+ T cells displayed only 2.15% ±1.34% of $ACE2^+$ cells (n = 11). The activated $CD8^+$HLA-DR^+ was only 2.72% ± 1.64% (n = 10) (Fig. 1f). We performed statistical analysis among different cell populations and found that the percentages of $ACE2^+$ NKT cells, activated $CD4^+$HLA-DR^+ T cells, activated $CD8^+$HLA-DR^+ T cells and $ACE2^+$ B cells were markedly higher than that of $CD4^+$ T cells ($P < 0.0001$, $P < 0.0001$, $P < 0.0001$, $P = 0.0015$ respectively) (Fig. 1f). However, there were no marked differences in the values of median fluorescence intensity (MFI) among different cell populations (Fig. 1g). The data suggests that SARS-CoV-2 virus may not directly attack blood immune cells lacking the ACE2 expression.

No expression of ACE2 on Th17 cells

T-helper type 17 (Th17) cells are important pathogenic mediators for several autoimmune diseases, potentially contributing to the pathogenesis of COVID-19. RORγt (retinoic acid receptor-related orphan nuclear receptor gamma t) belong to nuclear hormone receptors (NHRs) and act as a crucial transcription factor for the differentiation and function of Th17 cells both in humans and mice (24). Using RORγt, interleukin-17A (IL-17A), IL-17F, and CCR6 as specific Th17 markers (24), the purity of $IL17A^{+}ROR\gamma T^{+}$ Th17 cells was 19.91% ± 2.75% (Supplementary Figure 1a). The percentage of $IL17A^{+}IL17F^{+}$ Th17 cells was 20.19% ± 2.94% (Supplementary Figure 1a). The purity of $IL17A^{+}CCR6^{+}$ Th17 cells was 20.14% ± 2.86% (Supplementary Figure 1a). The gated Th17 cells failed to express ACE2 (Supplementary Figure 1b, 0.47% ± 0.65%, n = 4). This data implies no direct interaction between Th17 cells and SARS-CoV-2.

No expression of ACE2 on platelets

Increasing clinical evidence demonstrated the coagulation abnormalities in COVID-19 subjects including disseminated intravascular coagulopathy (DIC) and low levels of platelet count. To determine whether platelets were directly targeted by SARS-CoV-2 or trigged by viral inflammatory reactions, we examined the ACE2 expression on the highly-purified $CD41b^{+}CD42a^{+}$ platelets from human peripheral blood (Supplementary Figure 2a, n = 6). Flow cytometry established that there was no ACE2 expression on platelets (Supplementary Figure 2b and c, 0.58% ± 0.42%, n = 6), highlighting that the coagulopathy may be indirectly caused by the viral inflammation.

Our previous work established that platelets could release mitochondria contributing to the

immune modulation and islet β-cell regeneration (25). To explore the mitochondrial function in viral infection, flow cytometry indicated that while the purified platelet-derived mitochondria did not express ACE2 (Supplementary Figure 2d), they strongly display the mitochondrial antiviral-signaling protein (MAVS) with the percentage of MitoTracker Deep $Red^{+}HSP60^{+}MAVS^{+}$ mitochondria at 96.02% ± 2.74% (Supplementary Figure 2e, n = 3). This data suggests that platelets may have potential to improve antiviral immunity through the releasing mitochondria.

High expression of ACE2 on the activated type 1 macrophages (M1)

Macrophages have been characterized with type 1 macrophages (M1, inflammatory) and type 2 macrophages (M2, anti-inflammatory), according to their phenotypic differences such as spindle-like morphology and high expression CD206 and CD209 on M2 macrophages (15). Initially, flow cytometry established that the purified $CD14^{+}$ monocytes from human peripheral blood failed to express ACE2 (1.56% ± 1.91%, n = 6) (Fig. 2a). Macrophages were then generated in the presence of 50 ng/mL macrophage colony-stimulating factor (M-CSF) with the percentage of spindle-like cells at 63.25% ± 8.85% (n = 4). To evaluate the ACE2 expressions on macrophages, M1 and M2 macrophages were activated by the treatment with lipopolysaccharide (LPS) (14) and interleukin-4 (IL-4) respectively (21). Phase contrast image showed significant differences in the morphology between two groups (Fig. 2b). LPS-treated M2 macrophages exhibited pseudopod-like protrusions compared to the spindle form of IL-4-treated M2 macrophages (Fig. 2b). Phenotypic characterization established that up-regulations of CD206 and CD209 on the IL-4-treated M2 macrophages, not on the LPS-treated M1 macrophages (Fig. 2c). Flow cytometry demonstrated that the level of ACE2 expression was higher on the LPS-activated M1 macrophages than that of IL-4-treated M2 macrophages (Figs. 2d-f). This finding was further

confirmed by the confocal microscopy and image analysis (Fig. 2g). Therefore, the data suggests the upregulation of ACE2 expression on the activated M1 macrophages.

Expression of ACE2 on tissue macrophages

To detect the expression of ACE2 on tissue macrophages, we initially performed double-staining with human macrophage marker CD11b through the immunohistochemistry in the brain, lung, liver, kidney, and spleen tissues of normal adult human donors. Using an expression of ACE2 in the kidney as a positive control (Fig. 3a, 5th panel), the data revealed that most ACE2 expressions were co-localized with the CD11b^{+} tissue macrophages in the brain, lung and liver (Fig. 3a), which are known as microglia in brain (Fig. 3a, top panel), dust cells (alveolar macrophages, Fig. 3a, 2nd and 3rd panels) and Kupffer cells (Fig. 3a, 4th panel) respectively. Most splenocytes failed to exhibit ACE2 (Fig. 3a, 6th panel). Unexpectedly, there was little to no expression of ACE2 on the alveolar epithelial cells (Fig. 3a, 2nd and 3rd panels).

To further detect the distribution of ACE2 expression on alveolar epithelial cells, we utilized the primary human pulmonary alveolar epithelial cells (HPAEpiC) to define their level of ACE2 expression. Flow cytometry proved the low level (9%) of ACE2 expression on human pulmonary alveolar epithelial cells (Fig. 3b). Therefore, these data indicate the high expression of ACE2 on tissue macrophages with low level ACE2 expression on alveolar epithelial cells.

DISCUSSION

The human pulmonary system is primarily targeted by SARS-CoV-2. Our current studies demonstrated little to no expression of ACE2 on both primary human pulmonary alveolar epithelial cells and alveolar epithelial cells of paraffin lung tissue sections, which is consistent

with previous reports (8). Notably, we found that high expression of ACE2 was colocalized with human tissue macrophages of the lung (alveolar macrophages) and liver (Kupffer cells) and microglial cells in brain at steady state, and up-regulated on the LPS-activated M1 macrophages. However, most immune cells in the steady-state human peripheral blood samples were negative for ACE2 expression, including the freshly-isolated $CD14^+$ monocytes. It implies that the circulating monocytes may differentiate into alveolar macrophages after migration into the pulmonary tissues with an up-regulation of ACE2 expression. These alveolar macrophages act as the front line immune cells defending against the SARS-CoV-2 viral infection. These data highlight the importance of alveolar macrophages during the pathogenesis of lung damage in COVID-19 subjects. Liao et al. reported that there were abundant proinflammatory macrophages in the bronchoalveolar lavage fluid of severe COVID-19 patients (26). Additionally, Feng et al. reported that the viral nucleocaspid protein (NP) of SARS-CoV-2 was found in $ACE2^+CD169^+$ macrophages, but not in $CD3^+$ T cells and $B220^+$ B cells through postmortem examinations of COVID-19 patients' spleens and lymph nodes (27). Based on these evidence, we propose that lung macrophages may be directly targeted by the SARS-CoV-2 and play a critical role in the initiation and development of COVID-19 (Figure 4). Post viral infection, the SARS-CoV-2 may either (1) be directly cleared by the healthy macrophages with asymptomatic or mild clinical symptoms or (2) destroy the dysfunctional macrophages and evoke the immune system with cytokine storm, leading to severe clinical symptoms such as high fever, hypoxia and acute respiratory distress syndrome (ARDS) (Figure 4). This perspective may advance the understanding of the clinical course of COVID-19 and facilitate the development of prevention and treatment strategies.

Recently, Ural et al. (2020) reported that alveolar macrophages displayed the phenotype of type 1 macrophages (28), while an interstitial subset of $CD169^{+}$ lung-resident macrophages, primarily located around the airways in close proximity to the sympathetic nerves of the bronchovascular bundle, exhibit the characteristics of type 2 macrophages and anti-inflammatory effects (28). Therefore, these two types of macrophages play an essential role in the immune surveillance and maintenance of homeostasis of the pulmonary system. Considering all current approaches for the prevention and treatment of COVID-19, there are no therapies, either being tested or at the beginning of the pipeline, that directly focus on the modulation of macrophages. To this respect, it is critical to protect and restore the functions of alveolar macrophages (or other tissue macrophages) through immune modulations for the prevention and treatment of COVID-19, leading to being potentially beneficial to correct the viral inflammation, effectively ameliorate anti-viral immunity, efficiently reduce the viral load, improve clinical outcomes, expedite the patient recovery, and decline the rate of mortality in patients after being infected with SARS-CoV-2.

ACKNOWLEDGMENTS

Authors are grateful to Mr. Poddar and Mr. Ludwig for generous funding support via Hackensack UMC Foundation (No. 8061). All human buffy coat blood units and apheresis platelets were purchased from the New York Blood Center (NYBC, New York, NY). NYBC has received all accreditations for blood collections and distributions including the approval of Institution Review Board (IRB) and the signed Consent Forms from donors. Paraffin tissue sections were purchased from Biochain Institute (Newark, CA, USA) that has the ethical approvals for collections and distributions.

DISCLOSURE OF CONFLICTS OF INTEREST

All authors have no conflict of interest.

References:

1. Wrapp D, Wang N, Corbett KS, Goldsmith JA, Hsieh CL, Abiona O, et al. Cryo-EM structure of the 2019-nCoV spike in the prefusion conformation. Science. 2020;367(6483):1260-3.
2. Hoffmann M, Kleine-Weber H, Schroeder S, Kruger N, Herrler T, Erichsen S, et al. SARS-CoV-2 Cell Entry Depends on ACE2 and TMPRSS2 and Is Blocked by a Clinically Proven Protease Inhibitor. Cell. 2020;181(2):271-80 e8.
3. Ulrich H, Pillat MM. CD147 as a Target for COVID-19 Treatment: Suggested Effects of Azithromycin and Stem Cell Engagement. Stem cell reviews and reports. 2020;16(3):434-40.
4. Kim CH. SARS-CoV-2 Evolutionary Adaptation toward Host Entry and Recognition of Receptor O-Acetyl Sialylation in Virus-Host Interaction. International journal of molecular sciences. 2020;21(12).
5. Ulrich H, Pillat MM, Tarnok A. Dengue Fever, COVID-19 (SARS-CoV-2), and Antibody-Dependent Enhancement (ADE): A Perspective. Cytometry A. 2020;97(7):662-7.
6. Vankadari N, Wilce JA. Emerging WuHan (COVID-19) coronavirus: glycan shield and structure prediction of spike glycoprotein and its interaction with human CD26. Emerg Microbes Infect. 2020;9(1):601-4.
7. Sungnak W, Huang N, Becavin C, Berg M, Queen R, Litvinukova M, et al. SARS-CoV-2 entry factors are highly expressed in nasal epithelial cells together with innate immune genes. Nat Med. 2020;26(5):681-7.
8. Hikmet F, Mear L, Edvinsson A, Micke P, Uhlen M, Lindskog C. The protein expression profile of ACE2 in human tissues. Mol Syst Biol. 2020;16(7):e9610.
9. Hamming I, Timens W, Bulthuis ML, Lely AT, Navis G, van Goor H. Tissue distribution of ACE2 protein, the functional receptor for SARS coronavirus. A first step in understanding SARS pathogenesis. J Pathol. 2004;203(2):631-7.

10. Zhao Y, Zhao Z, Wang Y, Zhou Y, Ma Y, Zuo W. Single-Cell RNA Expression Profiling of ACE2, the Receptor of SARS-CoV-2. Am J Respir Crit Care Med. 2020;202(5):756-9.
11. Ding Y, He L, Zhang Q, Huang Z, Che X, Hou J, et al. Organ distribution of severe acute respiratory syndrome (SARS) associated coronavirus (SARS-CoV) in SARS patients: implications for pathogenesis and virus transmission pathways. J Pathol. 2004;203(2):622-30.
12. Mehta P, McAuley DF, Brown M, Sanchez E, Tattersall RS, Manson JJ, et al. COVID-19: consider cytokine storm syndromes and immunosuppression. Lancet. 2020;395(10229):1033-4.
13. Yao XH, Li TY, He ZC, Ping YF, Liu HW, Yu SC, et al. [A pathological report of three COVID-19 cases by minimal invasive autopsies]. Zhonghua Bing Li Xue Za Zhi. 2020;49(5):411-7.
14. Zhao Y, Glesne D, Huberman E. A human peripheral blood monocyte-derived subset acts as pluripotent stem cells. Proc Natl Acad Sci U S A. 2003;100(5):2426-31.
15. Hu W, Song X, Yu H, Sun J, Zhao Y. Released Exosomes Contribute to the Immune Modulation of Cord Blood-Derived Stem Cells. Front Immunol. 2020;11:165.
16. Yu H, Hu W, Song X, Descalzi-Montoya D, Yang Z, Korngold R, et al. Generation of Hematopoietic-Like Stem Cells from Adult Human Peripheral Blood Following Treatment with Platelet-Derived Mitochondria. International journal of molecular sciences. 2020;21(12).
17. Yu H, Hu W, Song X, Zhao Y. Generation of Multipotent Stem Cells from Adult Human Peripheral Blood Following the Treatment with Platelet-Derived Mitochondria. Cells. 2020;9(6).
18. Anderson RD, Haskell RE, Xia H, Roessler BJ, Davidson BL. A simple method for the rapid generation of recombinant adenovirus vectors. Gene Therapy. 2000;7(12):1034-8.
19. Jia HP, Look DC, Shi L, Hickey M, Pewe L, Netland J, et al. ACE2 receptor expression and severe acute respiratory syndrome coronavirus infection depend on differentiation of human airway epithelia. J Virol. 2005;79(23):14614-21.
20. Sun J, Zhuang Z, Zheng J, Li K, Wong RL, Liu D, et al. Generation of a Broadly Useful Model for COVID-19 Pathogenesis, Vaccination, and Treatment. Cell. 2020;182(3):734-43 e5.
21. Bertani FR, Mozetic P, Fioramonti M, Iuliani M, Ribelli G, Pantano F, et al. Classification of M1/M2-polarized human macrophages by label-free hyperspectral reflectance confocal microscopy and multivariate analysis. Scientific reports. 2017;7(1):8965.
22. Zhao Y, Lin B, Darflinger R, Zhang Y, Holterman MJ, Skidgel RA. Human cord blood stem cell-modulated regulatory T lymphocytes reverse the autoimmune-caused type 1 diabetes in nonobese diabetic (NOD) mice. PLoS ONE. 2009;4(1):e4226.
23. Maecker HT, McCoy JP, Nussenblatt R. Standardizing immunophenotyping for the Human Immunology Project. Nat Rev Immunol. 2012;12(3):191-200.
24. Huh JR, Littman DR. Small molecule inhibitors of RORgammat: targeting Th17 cells and other applications. Eur J Immunol. 2012;42(9):2232-7.
25. Zhao Y, Jiang Z, Delgado E, Li H, Zhou H, Hu W, et al. Platelet-Derived Mitochondria Display Embryonic Stem Cell Markers and Improve Pancreatic Islet beta-cell Function in Humans. Stem Cells Transl Med. 2017;6(8):1684-97.

26. Liao M, Liu Y, Yuan J, Wen Y, Xu G, Zhao J, et al. Single-cell landscape of bronchoalveolar immune cells in patients with COVID-19. Nat Med. 2020.
27. Feng Z, Diao B, Wang R, Wang G, Wang C, Tan Y, et al. The Novel Severe Acute Respiratory Syndrome Coronavirus 2 (SARS-CoV-2) Directly Decimates Human Spleens and Lymph Nodes. medRxiv. 2020:https://doi.org/10.1101/2020.03.27.20045427.
28. Ural BB, Yeung ST, Damani-Yokota P, Devlin JC, de Vries M, Vera-Licona P, et al. Identification of a nerve-associated, lung-resident interstitial macrophage subset with distinct localization and immunoregulatory properties. Sci Immunol. 2020;5(45).

Figure Legends:

Fig. 1. Examination of ACE2 expression on different types of immune cells. Human peripheral blood mononuclear cells (PBMC) were isolated from healthy donors (n = 14) with Ficoll-Paque Plus (γ = 1.077). Red blood cells were removed using ACK lysis buffer. The remaining PBMC were utilized for flow cytometry. (**a – c**) Gating strategies of flow cytometry analysis for different types of immune cells including (**a**) $CD3^+CD4^+$ T cells, $CD3^+CD8^+$ T cells, $CD4^+CD25^+CD127^{low/-}$ Treg, $CD3^-CD56^+$ NK, $CD3^+CD56^+$ NKT cells, (**b**) $CD3^-CD19^+$ B cells, $CD3^-CD14^+$ monocytes (Mo), $CD14^-CD11c^+$ myeloid dendritic cells (mDC), $CD14^-CD123^+$ plasmacytoid dendritic cells (pDC), and $CD3^-CD66b^+$ granulocytes (Gr), (**c**) activated $CD4^+$HLA-DR^+ T cells and activated $CD8^+$HLA-DR^+ T cells. (**d**) Flow cytometry shows the ACE2 expression on the Ad5-hACE2-transfected 293T cells. IgG served as negative control. Representative data of those obtained from three experiments. (e) ACE2 expression on different compartments of immune cells. (f) Little to no expressions of ACE2 on different gated subsets of

immune cells by flow cytometry. Isotype-matched IgGs served as negative controls. (g) Median fluorescence intensity (MFI) of ACE2 expressions on different compartments of immune cells. Data are presented as mean ± SD.

Fig.2. Different levels of ACE2 expressions on M1 and M2 macrophages. (**a**) The freshly-purified $CD14^+$ monocytes from human peripheral blood failed to express ACE2. Isotype-matched IgG served as control. (**b – g**) The purified $CD14^+$ monocytes were initially seeded in the tissue culture-treated 6-well plate at 5×10^5 cells/well and cultured in X-VIVO 15 serum-free media with 50 ng/mL M-CSF (14), at 37 °C, 5% CO_2 conditions. After 7 days, M2 macrophages were treated with 1 μg/mL LPS or 40 ng/mL IL-4 for 24 hours respectively. (**b**) Morphological change of M2 macrophages after the treatment LPS (N = 4, left). IL-4-treated macrophages served as control with maintaining the morphology of spindle-like cells (right). (c) Phenotypic characterization of M1/M2 with their associated markers. Isotype-matched IgGs served as negative controls. Data were representative from one of two PBMC preparations. (**d**) Overlay histogram shows the high expression of ACE2 on M1 macrophages (red) in comparison with M2 macrophages (green). The isotype 2^{nd} Ab staining served as negative control (grey). (**e**) M1 macrophages display higher percentage of $ACE2^+$ cells than that of M2 macrophages. Data are presented as mean ± SD. N = 3. (**f**) M1 macrophages display higher level of ACE2 median fluorescence intensity (MFI) than that of M2 macrophages. Data are presented as mean ± SD. N = 3. (**g**) Fluorescence microscopy shows high expression of ACE2 on M1 macrophages. Representative images were from one of immunostaining with six experiments.

Fig. 3. Expression of ACE2 on human tissue macrophages. (**a**) Expression of ACE2 was co-

localized with the $CD11b^+$ tissue macrophages (pointed by yellow triangles) in the brain, lung and liver, which are known as microglia in brain (top panel), dust cells (alveolar macrophages, 2^{nd} and 3^{rd} panels) and Kupffer cells (4^{th} panel) respectively. There was little to no expression of ACE2 on alveolar epithelial cells. Paraffin tissue sections were derived from normal adult human donors (Biochain Institute). Tissue sections stained with 2^{nd} Abs served as negative control. (**b**) Analysis of ACE2 expression on the primary human pulmonary alveolar epithelial cells (HPAEpiC) by flow cytometry. The 2^{nd} Ab staining served as negative control (grey) for ACE2 immunostaining (red). The total cell population (left panel) was gated for flow cytometry analysis.

Fig. 4. Outline the proposed mechanism underlying the pathogenesis of COVID-19. ACE2 protein was primarily displayed on alveolar macrophages of lung, with no or low expression on alveolar type 1 (AT-I) and type 2 (AT-II) epithelial cells. Upon entering the pulmonary alveoli, healthy alveolar macrophages may directly kill the virus, with asymptomatic or mild clinical symptoms. At this earlier stage 1, the infected alveolar macrophages may alternatively recruit other immune cells to build up the antiviral immunity through releasing cytokines (e.g., IL-1, IL-6, IL-12, and TNFα) and chemokines (e.g. CXCL1 and CXCL2 to recruit granulocytes, CXCL10 to recruit T cells, NK cells, and DCs). For instance, the recruited $CD4^+$ T cells may secret interferon (IFN)-γ to strengthen the antiviral immunity of alveolar macrophages and minimize the viral load. However, if this first line of defense is broken, the more cytokines and chemokines are released from the dead cells or dead-cell engulfed macrophages (Stages 2 and 3), the more immune cells are infiltrated into pulmonary systems, leading to patients experiencing a rapid deterioration and the development of ARDS with high fatality in the clinic.

Figure 1

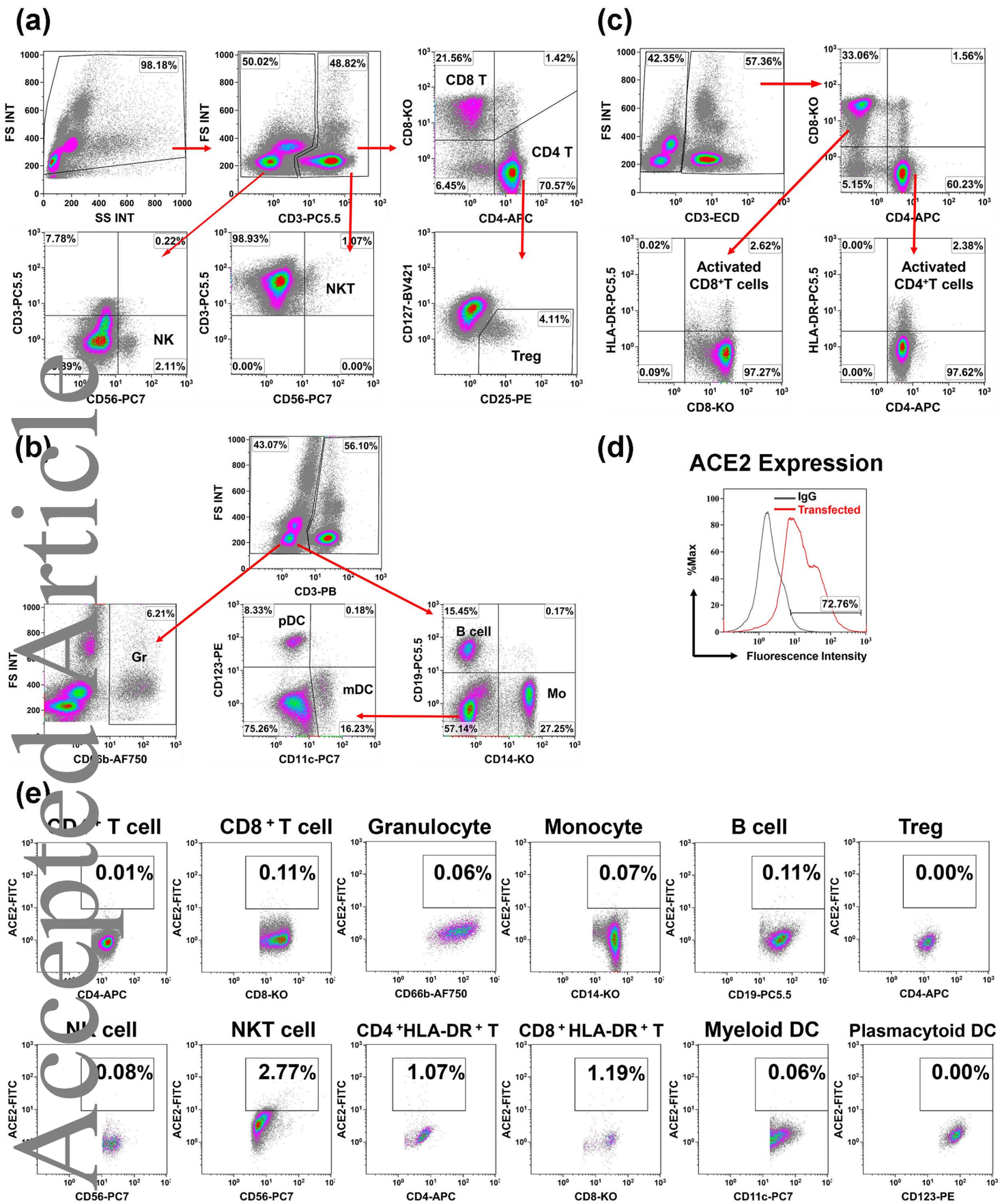

Figure 2

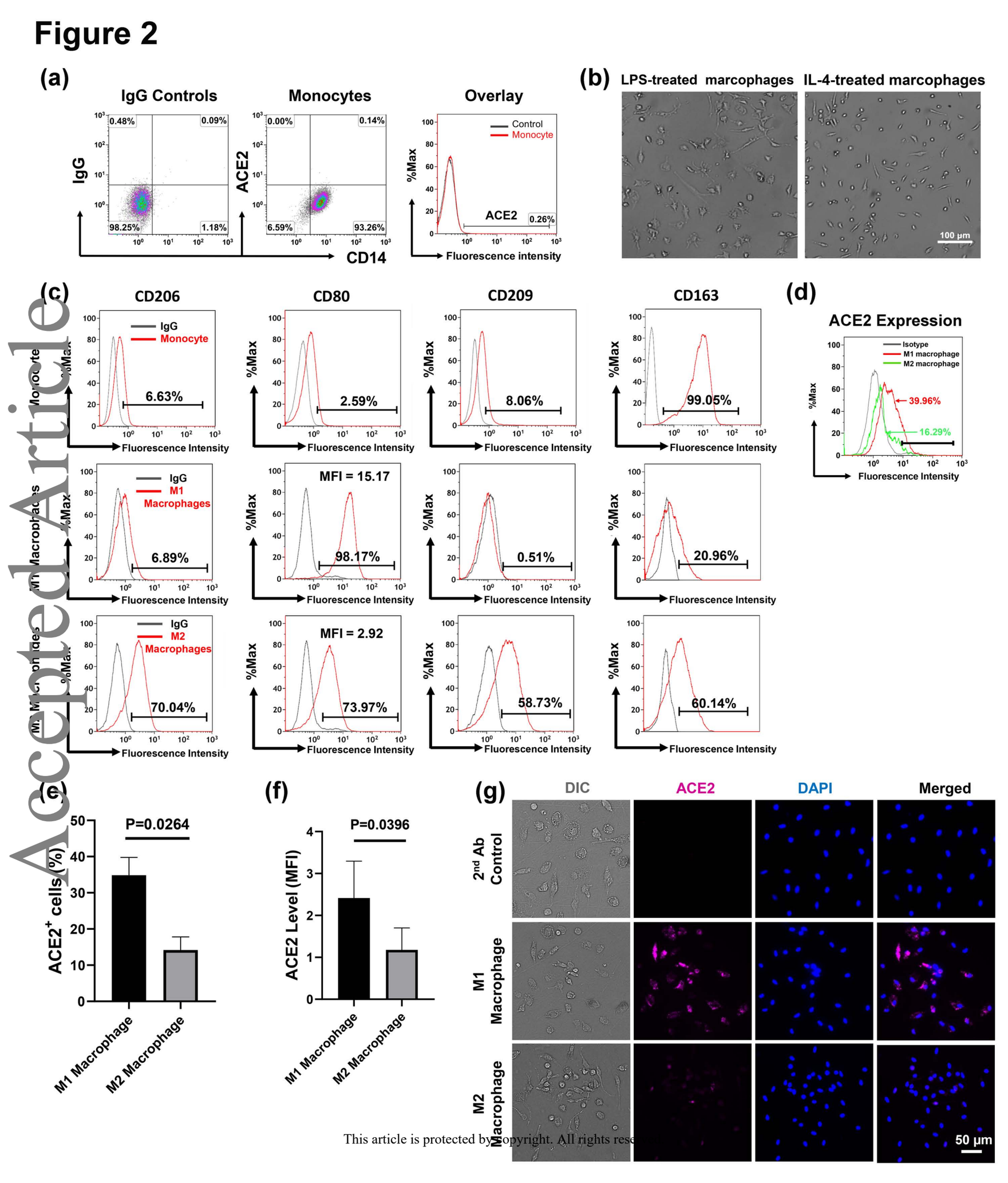

Figure 3